Revised July 16, 2001

A Lagrangian approach to studying Arctic polar stratospheric clouds using UARS MLS HNO_3 and POAM II aerosol extinction measurements

M. L. Santee,[1] A. Tabazadeh,[2] G. L. Manney,[1,3] M. D. Fromm,[4]
R. M. Bevilacqua,[5] J. W. Waters,[1] and E. J. Jensen[2]

Abstract. We assess the viability of diagnosing polar stratospheric cloud (PSC) composition and denitrification using existing satellite measurements. A Lagrangian approach is used to track PSC evolution from formation through dissipation. Upper Atmosphere Research Satellite Microwave Limb Sounder observations of gas-phase HNO_3 and Polar Ozone and Aerosol Measurement II observations of aerosol extinction from the Arctic late winter of 1995/1996 are correlated and compared to results from PSC composition models along air parcel trajectories. This approach is successful in capturing the broad patterns of PSC development. That is, a strong correlation is found between low-temperature, low-HNO_3, and high-extinction points. In most cases the observed behavior along the Lagrangian paths falls within the range predicted by equilibrium liquid ternary aerosol and nitric acid trihydrate composition models. At no time along the trajectories (when there is data coverage) do the models display large changes in either HNO_3 or aerosol extinction that are not reflected in the data. In general, however, there is a large degree of overlap in the comparisons between the models and the data. Unmeasured quantities and large uncertainties in both measurements and model calculations preclude conclusive determination of PSC composition or phase in most cases. In the majority of PSC events studied, gas-phase HNO_3 fully recovers to pre-PSC abundances following cloud evaporation. We conclude that, while severe denitrification (50% or greater) may have occurred in highly localized regions in the Arctic in 1996, it did not occur over spatial scales comparable to or larger than the MLS field of view ($\sim$400 km$\times$200 km$\times$6 km), even though it was a relatively cold winter. Improved measurements from upcoming satellite missions, such as Earth Observing System Aura, will ameliorate many of the difficulties in diagnosing PSC composition and denitrification encountered in this study.

1. Introduction

Understanding the phase and composition of polar stratospheric clouds (PSCs) is especially important in the Arctic, where the stratosphere is often only marginally cold enough to support PSCs now but where the frequency, extent, and duration of PSC events may increase under possibly colder and wetter conditions in the coming decades [e.g., *Waibel et al.*, 1999; *Tabazadeh et al.*, 2000]. Despite a considerable number of observational, laboratory, and modelling studies over the last 15 years, however, specific PSC formation mechanisms remain uncertain [for more complete surveys of PSC-related studies, see *Tolbert*, 1994; *Carslaw et al.*, 1997; *Peter*, 1997; *World Meteorological Organiza-*

[1]Jet Propulsion Laboratory, California Institute of Technology, Pasadena.
[2]NASA Ames Research Center, Moffett Field, California.
[3]Department of Natural Resources Management, New Mexico Highlands University
[4]Computational Physics, Inc., Fairfax, Virginia.
[5]Naval Research Laboratory, Washington, D. C.

tion, 1999; *Toon et al.*, 2000].

A recent thrust of in situ PSC studies in the Arctic has been to take a quasi-Lagrangian approach, whereby the aircraft flight path is directed parallel (or nearly so) to the wind at the level of the PSC [e.g., *Carslaw et al.*, 1998; *Wirth et al.*, 1999]. This allows measurements to be made along air parcel trajectories from the leading to the trailing edge of the cloud and, at least in principle, affords observation of the rapid microphysical processes occurring during the brief interval that air parcels spend within the cloud (although the transit time of an aircraft is considerably shorter than that of a typical air parcel).

A Lagrangian approach, similar to the Match technique for assessing chemical ozone depletion [*Rex et al.*, 1998], can also be applied to satellite measurements. *Steele et al.* [1999] were the first to employ multiple sampling of satellite aerosol measurements along air parcel trajectories to characterize cloud evolution. They tracked PSC development by comparing aerosol extinction spectra obtained by the Polar Ozone and Aerosol Measurement (POAM) II with results from a microphysical model at multiple points along air parcel trajectories, but they did not include HNO_3 sequestration in clouds in their analysis. *Danilin et al.* [2000] demonstrated a similar "trajectory hunting" approach by running a photochemical box model along trajectories of air parcels that had been sampled multiple times by the Microwave Limb Sounder (MLS) and Cryogenic Limb Array Etalon Spectrometer (CLAES) instruments onboard the Upper Atmosphere Research Satellite (UARS). The focus of their study, however, was chlorine activation, and they did not find measurements of chlorine species useful in distinguishing between different PSC compositions since uncertainties are large and both solid and liquid PSCs produced comparable levels of reactive chlorine in the model. *Dessler et al.* [1999] examined MLS HNO_3 and CLAES aerosol extinction measurements from several northern hemisphere winters. Although their analysis was based on the calculation of trajectories and the identification of air parcels sampled multiple times, it did not involve following air parcels in an individual sense. Rather, it relied on averaging observations over the entire winter/early spring period and consequently provided no information on PSC evolution.

Here we investigate Arctic PSCs by applying a Lagrangian approach to UARS MLS measurements of gas-phase HNO_3 and POAM II measurements of aerosol extinction. By examining the same air parcels multiple times as they traverse regions of PSC activity, the complete cloud particle development along the trajectories can be followed. This study is the first to track PSC evolution, from formation through dissipation, by comparing observations of both gas-phase HNO_3 and aerosol extinction to model calculations along air parcel trajectories. Our main goal in this study is to assess the viability of diagnosing PSC composition and denitrification using existing satellite measurements. Although they lack the resolution and precision of in situ measurements, the satellite measurements have the important advantage of providing daily or near-daily coverage over a range of pressures. Thus a number of PSC events can be studied over the course of the winter. If conclusive identification of PSCs can be made, a substantial set of statistics on PSC development and evolution can be compiled over the lifetime of the two instruments.

2. Measurement Description

2.1. UARS Microwave Limb Sounder (MLS)

The microwave limb sounding technique and the MLS instrument are described in detail by *Waters* [1993] and *Barath et al.* [1993], respectively. Because long wavelengths are used, the data are not degraded by the presence of PSCs or other stratospheric aerosols [see *Waters et al.*, 1999, Figure 3]. The latitudinal coverage of MLS measurements extends from 80° on one side of the equator to 34° on the other. Roughly every 36 days (a "UARS month"), MLS alternates between viewing northern and southern high latitudes.

Santee et al. [1996] presented version 4 HNO_3 data for the 1995/1996 Arctic winter studied here, and *Santee et al.* [1998] presented version 4 HNO_3 data from the 1992–1996 Antarctic winters and specifically addressed their suitability for use in studies of PSC composition. Results shown in this paper are from the recently-released version 5 MLS retrieval algorithms, in which the HNO_3 retrievals have been significantly improved. In version 5 geophysical parameters are retrieved on every UARS surface (six surfaces per decade in pressure, as opposed to three in previous MLS data sets), although the actual vertical resolution of the data has not doubled. Preliminary validation studies indicate that the version 5 MLS HNO_3 data are scientifically useful over the range 100–4.6 hPa, with the estimated precision for an individual profile between 0.9 and 1.9 ppbv throughout this domain. The uncertainties consist of both random and systematic components, but the random (noise) components usually dominate for the MLS HNO_3 measurement. Many of the results shown in this study have been derived through averaging several individual data points and therefore (since averaging reduces the noise contribution to the uncertainty) have better precision ($<$1.0 ppbv). Further details of the quality of the MLS version 5 data are available from the MLS web site (http://mls.jpl.nasa.gov).

The retrieved version 5 MLS HNO_3 values at a particular geographic location and atmospheric level represent averages over a $\sim$400 km$\times$200 km$\times$6 km volume of air. Al-

though both crystalline and liquid PSCs routinely extend continuously over spatial scales comparable to or larger than the MLS footprint [*World Meteorological Organization*, 1999; *Toon et al.*, 2000], it is possible that multiple cloud types could exist within the volume of air sensed by MLS. This is particularly true in the Arctic, where the low temperatures are often confined to relatively small regions. *Hervig et al.* [1997] discuss the inherent limitations in using satellite limb observations [in particular from UARS Halogen Occultation Experiment (HALOE)] arising from the possibility of cloud inhomogeneity over the sample volume. For the purposes of this investigation, we have assumed that any PSCs present are uniform over the MLS field of view.

2.2. Polar Ozone and Aerosol Measurement (POAM)

POAM II used a solar occultation technique to measure the vertical distribution of atmospheric constituents and aerosol extinction with a vertical resolution of about 1 km and a horizontal resolution of about 200×30 km [*Glaccum et al.*, 1996]. In normal operation, POAM recorded 12–13 occultation events per day around a circle of latitude in each hemisphere, with successive occultations separated by $\sim 25^\circ$ in longitude. During the period studied here, the latitude of the northern hemisphere (satellite sunrise) measurements varied between about 66° and 68°N.

The 1.06 μm channel is the primary channel for PSC detection. *Lumpe et al.* [1997] discuss in detail the version 5 POAM retrieval algorithm and error analysis; they estimate random errors in the retrieved aerosol extinction to be 10–20% for the 1.06 μm channel. Several different validation efforts have shown good agreement between the POAM aerosol extinction profiles and those from other instruments [*Randall et al.*, 1996, 2000; *Brogniez et al.*, 1997; *Fromm et al.*, 1997]. In particular, *Randall et al.* [2000] perform a statistical comparison of coincident version 6 POAM and version 5.931 Stratospheric Aerosol and Gas Experiment (SAGE) II summertime extinction profiles and find differences in the 1 μm measurements to be within ±10% between 12 and 27 km. Here we use version 6 data.

Fromm et al. [1997, 1999] describe the POAM cloud detection algorithm used to distinguish PSCs from the background aerosol. Two distinct PSC signatures are evident in the POAM data; these are referred to as "layer" and "high Zmin" PSCs. Layer PSCs are identified when the extinction ratio profile, defined as the 1.06 μm aerosol extinction divided by a representative cloudless-air profile, exhibits a local maximum that exceeds a certain threshold value. Low, middle, and high threshold enhancements are assigned codes of "1", "2", and "3", respectively. Occasionally a cloud is observed that is so optically thick that the radiance incident on the instrument's sun tracker drops below the detection threshold; this causes the occultation event to be terminated at an anomalously high tangent altitude and is therefore labelled as a "high Zmin" PSC. *Fromm et al.* [1999] argue that most of the high Zmin cases are indicative of water ice clouds; this view is supported by the recent analysis (of POAM III data) by *Nedoluha et al.* [2000]. The POAM PSC categories are employed in the analysis here only to aid in the selection of the particular occultation events for which trajectories are launched; all of our interpretations regarding PSC types are based on the model comparisons described in section 4.

3. Overview of Coincident Measurements

The data coverage of the POAM II and MLS instruments overlapped for three northern hemisphere winters: 1993/1994, 1994/1995, and 1995/1996. POAM operated only sporadically during the 1993/1994 Arctic PSC season, however, and the POAM extinction values at this time were significantly higher than in subsequent years because of residual aerosol loading from the eruption of Mt. Pinatubo [*Randall et al.*, 1996], complicating PSC identification [*Fromm et al.*, 1999]. In addition, the 1993/1994 winter was relatively warm, with minimum temperatures at 465 K near or above the average for the last 20 years for most of the season [*Zurek et al.*, 1996]. Thus the number of POAM PSC detections during this winter is limited [*Fromm et al.*, 1999]. POAM operated continuously during the 1994/1995 winter, which was considerably colder, but MLS data collection during this period was severely restricted because of difficulties with the MLS scan system and the spacecraft batteries and solar array. As a result, a complete PSC lifecycle was not captured in the 1994/1995 MLS data.

We focus here on the 1995/1996 Arctic late winter period winter. With the exception of 1999/2000, the 1995/1996 winter was the coldest, the most persistently cold, and cold over the largest geographical area, of any northern winter in the meteorological data record for the past ∼40 years [*Manney et al.*, 1996a; *Naujokat and Pawson*, 1996; *Pawson and Naujokat*, 1999]. Daily minimum temperatures inside the vortex at 465 K were below 195 K, the approximate existence threshold for nitric acid trihydrate (NAT) PSCs, for 80 consecutive days, and below 188 K, the nominal ice frost point for lower stratospheric conditions, for a total of 28 days [*Manney et al.*, 1996a]. Thus meteorological conditions were conducive to abundant PSC formation, and POAM observed PSCs almost daily between mid-December and early March [*Fromm et al.*, 1999]. By 1996 MLS was operated only intermittently, to conserve both spacecraft power and

instrument lifetime. During the late winter north-looking period from January 26 to March 5, 1996, MLS made measurements on a total of 17 days. In this section we present an overview of coincident MLS and POAM observations during this period and provide a meteorological context for them, setting the stage for the detailed trajectory analyses of section 4.

Plate 1 shows maps of MLS gas-phase HNO_3 for selected days in the late-winter north-looking period. The MLS data are gridded by binning and averaging 24 hours of data; the averages are then vertically interpolated to 465 K (ranging from ∼30 to 60 hPa for the low temperatures inside the polar vortex) using the U.K. Met Office (UKMO) [*Swinbank and O'Neill*, 1994] temperatures. Contours of UKMO temperature and potential vorticity (PV) are also shown. We concentrate on the 465-K level since it is often situated near the center of the maximum aerosol extinction. Wintertime gas-phase HNO_3 abundances are generally high in the warmer regions of the polar vortex, as a result of confined diabatic descent, but low in the colder regions, where PSCs form. The locations of the POAM occultations on each day are also overlaid on the maps, with different symbols representing different PSC detection categories (see section 2.2). On any given day, the majority of the POAM measurements indicate cloudless-air extinction values. As can be seen from Plate 1, overall there is good agreement between POAM PSC detections and depleted MLS gas-phase HNO_3.

Minimum temperatures at 465 K were near or below 188 K in mid-January, but had begun to warm up slightly at the beginning of the MLS north-looking period in late January [*Manney et al.*, 1996a]. The MLS observations at the end of January were followed by a data gap until February 13, by which time a small pocket of temperatures below the frost point had developed northeast of Iceland. POAM observed a high Zmin PSC in this region, which was also where the MLS HNO_3 values were lowest. Extremely cold conditions continued to prevail throughout the lower stratosphere over the course of the next week. *Fromm et al.* [1999] showed that the numerous high Zmin events recorded between February 13 and February 21 were consistent with the presence of water ice PSCs. They inferred the occurrence of a multi-day, synoptic-scale PSC episode with substantial HNO_3-containing and water ice cloud coverage during this period.

The meteorological conditions on February 20, 1996, were the most Antarctic-like observed by MLS during its entire lifetime to date, with 465-K minimum temperatures inside the polar vortex approaching those of a typical southern winter [*Manney et al.*, 1996a]. On this day a strong tropospheric anticyclone resulted in the deformation of the lower stratospheric vortex and caused the region of lowest temper-

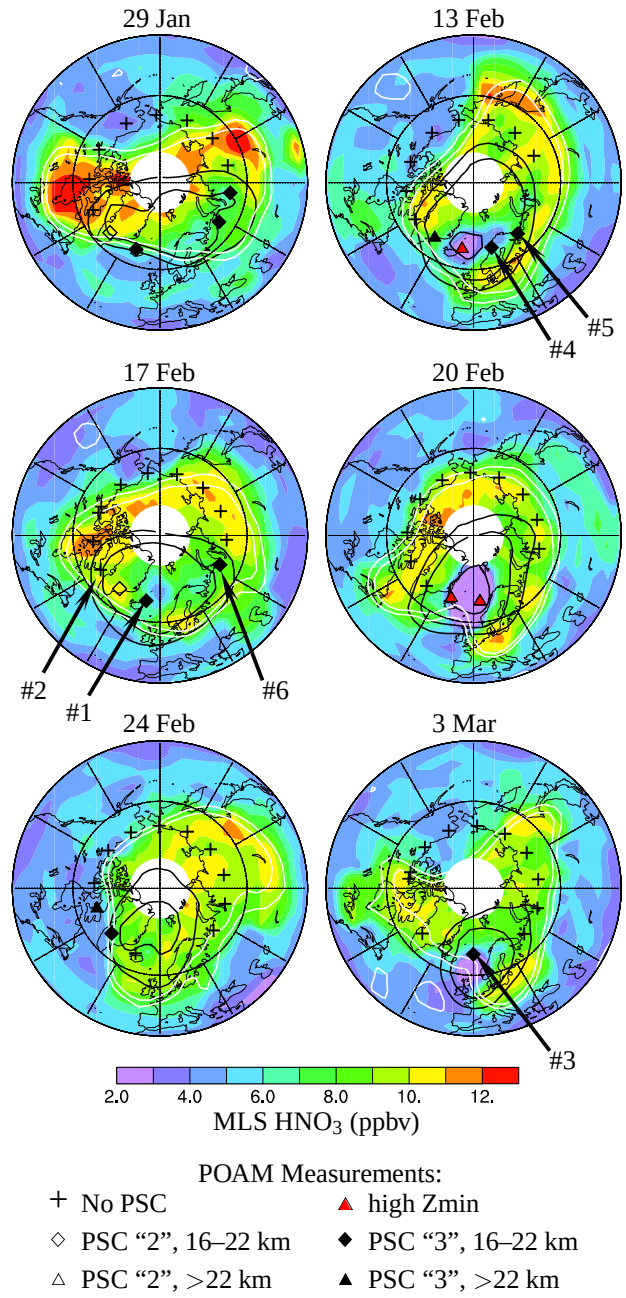

Plate 1. Maps of MLS HNO_3 for selected days during the 1995/1996 late northern winter north-viewing period, interpolated to 465 K using UKMO temperatures. The maps are polar orthographic projections extending to the equator, with the Greenwich meridian at the bottom and dashed black circles at 30°N and 60°N. Superimposed in white are two contours of UKMO potential vorticity (PV): 0.25×10^{-4} K m^2 kg^{-1} s^{-1} (to represent the approximate edge of the winter polar vortex at this level) and 0.30×10^{-4} K m^2 kg^{-1} s^{-1} (a second contour to indicate the steepness of the PV gradient and thus the strength of the vortex). Superimposed in black are three contours of UKMO temperature: 200 K, 195 K, and 188 K. The locations of the POAM occultations on each day are also overlaid. Cloudless-air extinction values are represented by plus signs. PSC events for which the extinction enhancement exceeded the high threshold, category "3", are depicted by filled black symbols; possible layer PSCs, for which the extinction enhancement exceeded the middle threshold, category "2", are depicted by open symbols. For both PSC designations, diamonds represent peak extinction enhancement in the 16–22 km range, which straddles the 465-K surface on which MLS data are shown. Layer PSCs at higher altitudes are represented by triangles; PSC detections whose peak layer occurred below 16 km are ignored. High Zmin cases are shown as filled red triangles. Arrows mark the individual occultation events examined in detail in section 4.

atures to be situated very near the vortex edge [*Manney et al.*, 1996a]. *Santee et al.* [1996] used high-resolution three-dimensional transport calculations to show that the observed HNO_3 decrease was not a consequence of the entrainment of lower-latitude air into the vortex. A similar investigation of a second strong tropospheric anticyclone also concluded that the HNO_3 depletion observed on March 3 arose from PSC activity and not dynamical processes [*Santee et al.*, 1996].

4. Trajectory Analysis of PSC Evolution

Several of the PSC episodes shown in the maps in Plate 1 will now be examined in detail. We combine the HNO_3 and aerosol extinction data in a Lagrangian approach that entails following air parcels in the days just before and after POAM occultation events and comparing the observed HNO_3 and aerosol extinction behavior along their paths with that predicted by PSC composition models. In this section we assess the viability of determining the composition of the clouds formed during individual PSC events using existing satellite measurements, taking into account various significant uncertainties in both measurements and models.

4.1. Approach

Thermal histories of observed air parcels are obtained by performing 5-day trajectory calculations both backward and forward from POAM occultation events. The three-dimensional trajectory code, described by *Manney et al.* [1994], is run using horizontal winds and temperatures from UKMO analyses. For each trajectory, 25 parcels are initialized in a $0.5^\circ \times 1^\circ$ latitude/longitude ($\sim 50 \times 50$ km) box centered on a POAM occultation point. In none of the PSC cases shown here did the parcels display a large degree of dispersion; the maximum difference in temperature along the various parcel trajectories at any timestep was about 5 K and most differences were much smaller. Thus the whole ensemble is represented well by the central parcel, and only its coordinates are actually followed in this study. Both backward and forward trajectory calculations are started at the potential temperature level corresponding to the peak in the POAM extinction profile. For those cases when no extinction enhancement was detected, 465 K is used as the default level for the trajectory initialization. The parcels typically undergo diabatic descent of approximately 10–20 K over the 10 days total represented in these runs, depending on the initialization altitude. The initialization time of the trajectory is set to the nearest half-hour (the trajectory timestep) to the occultation time. Temperature histories are constructed by interpolating UKMO temperatures to the time, latitude, longitude, and potential temperature values of the central parcel along the combined 10-day trajectory.

Estimates of measured values along the trajectory are obtained in a two-part process at each timestep. First, the data are vertically interpolated onto the parcel potential temperature surface. Next, a gridding procedure is applied wherein an average is computed with MLS observations weighted by their distance in space and time from the air parcel location at that timestep. The gridding is not especially sensitive to the shape of the weighting function; here we used a $\cos^2$ function. The halfwidth values, chosen in keeping with the MLS data sampling, are 2° in latitude, 7° in longitude, and 12 hours. Only data within one halfwidth of the trajectory position are included. These values permit a few data points at most to contribute to the average, thus minimizing the effects of smoothing while still allowing more than one MLS measurement recorded close to the trajectory at a given timestep to influence the estimated HNO_3 value there. If no measurements fall within the prescribed distance in space and time, then the gridding routine returns a missing data value. Because of the orbit track spacing, the along-track resolution, the timing of the measurements, and the occasional gaps in measurement coverage, estimates of MLS data are not available at every timestep. Furthermore, because the trajectory timestep is much smaller than the time halfwidth used in the gridding procedure, the gridded data tend to become available in short clumps along the trajectory. A similar procedure is applied to the POAM data, but the number of trajectory timesteps with coincident POAM measurements is smaller than for MLS.

To compare with the observations, equilibrium composition models are used to compute HNO_3 vapor pressure and aerosol volume at each timestep along the combined 10-day trajectory assuming nitric acid trihydrate (NAT) [*Hanson and Mauersberger*, 1988] and liquid ternary aerosol (LTA) [*Tabazadeh et al.*, 1994b] phases. The various model parameters for the standard runs are summarized in Table 1, and sensitivity tests exploring variations in these parameters are listed in Table 2. Unfortunately, no simultaneous colocated measurements of water vapor are available. However, MLS measurements from previous Arctic winters indicate that in mid-February neither the horizontal nor the vertical gradients in H_2O are particularly strong inside the lower stratospheric vortex, and 5 ppmv is a reasonable estimate for the H_2O mixing ratio, except in the coldest regions where water ice PSCs may be forming. This value is in agreement with measurements of H_2O inside the vortex from aircraft over the range 370 K to 470 K during the Airborne Arctic Stratospheric Expedition (AASE) [*Kelly et al.*, 1990] and from balloons over the range 450 K to 550 K during the European Arctic Stratospheric Ozone Experiment (EASOE) [*Ovarlez and Ovarlez*, 1994]. In the absence of more specific information, we assume a constant H_2O mixing ratio of 5 ppmv

for the standard model runs at all levels. Since by 1996 the aerosol loading of the Arctic stratosphere had essentially returned to pre-Pinatubo conditions [*Thomason et al.*, 1997; *Deshler and Oltmans*, 1998], we use an H_2SO_4 mixing ratio of 0.2 ppbv to represent nonvolcanic background conditions [e.g., *Beyerle et al.*, 1997]. This value generally provides good agreement between the calculated extinctions and those obtained by POAM in warm regions well away from PSC activity. To reflect variations in the HNO_3 field around the vortex, the total amount of available HNO_3 is tuned to match the MLS observations along the back trajectory before significant PSC activity, typically by taking the MLS value at the closest point prior to the initialization time for which the temperature is above 205 K. If no such point exists along the back trajectory, then the total HNO_3 is set to 10 ppbv.

Aerosol volumes obtained from the equilibrium composition models are converted into extinction units using Mie calculations. A constant lognormal size distribution is assumed for the background aerosols (with a mode radius of 0.092 μm, a distribution width of 1.8, and a number concentration of 10 cm^{-3}), based on in situ measurements made during AASE [*Dye et al.*, 1992]. A constant refractive index of 1.6 is used for NAT [*Toon et al.*, 1990]. For LTA, a variable refractive index is calculated using the values for binary H_2SO_4/H_2O solutions tabulated by *Palmer and Williams* [1975]. *Luo et al.* [1996] compared refractive indices estimated for ternary solutions to those reported by *Palmer and Williams* [1975] for the binary system and found that the ternary values are up to 1.5% larger for temperatures in the range 185–195 K. A sensitivity test in which the refractive indices in our Mie code were increased by 1.5% resulted in reductions in the computed aerosol extinction of at most 5%. Therefore, the use of the refractive index data from *Palmer and Williams* [1975] should not have a significant effect on our modelled LTA extinctions. Because LTA droplets form from the background (liquid) sulfate aerosols via condensational growth (i.e., without a nucleation barrier), the mode radius of the size distribution simply shifts to a larger value. Thus LTA particles are characterized by a number concentration similar to, but a mode radius significantly (up to a factor of 4) larger than, the background aerosols [*Tabazadeh et al.*, 1994a]. In contrast, a nucleation step is required to form NAT from LTA. Since only a small fraction of LTA droplets are likely to overcome the nucleation barrier to form NAT particles, their number density is likely to be substantially smaller than that of the background or LTA particles. In fact, recent in situ observations [*Fahey et al.*, 2001] and theoretical calculations [*Tabazadeh et al.*, 2001] have suggested that synoptic-scale NAT clouds are composed of very few ($\sim 10^{-4}$ cm^{-3}), very large (5–10 μm radius) particles, although much higher number densities (0.1–1.0 cm^{-3}) of smaller NAT particles have been observed in mountain-wave clouds [*Carslaw et al.*, 1998; *Voigt et al.*, 2000]. Airborne lidar data obtained during January 1989 also suggest that clouds composed of very few, very large particles are widespread in the Arctic [*Toon et al.*, 2000]. For the large-scale PSCs observable in the satellite measurements, we assume a NAT number density of 10^{-4} cm^{-3} in the standard model runs. In calculating the extinction due to NAT, the number density is assumed fixed and the size of the particles is allowed to vary as the HNO_3 in excess of saturation varies. The calculated extinctions are, however, extremely sensitive to the assumed number density, and we explore variations in this parameter in a number of sensitivity tests (see Table 2).

4.2. Factors Complicating Data/Model Interpretation

In this section we discuss the various factors that might cause apparent discrepancies between the MLS and the POAM observations, and between both sets of observations and their associated model predictions. We performed several sets of sensitivity tests, listed in Table 2, to explore the influence of some of these factors on our results. Although most sensitivity tests were run for all cases shown here, they are reported in connection with individual cases only where appropriate.

Quantities such as the H_2O, H_2SO_4, and HNO_3 mixing ratios and the fraction of particles nucleated have a strong influence on the model results. It is possible to improve the agreement in most cases by tweaking various model parameters. The model calculations are also highly sensitive to temperature. *Manney et al.* [1996b] found that, compared to radiosondes, UKMO temperatures at northern polar latitudes in mid-February 1995 were systematically high by almost 2.5 K, with occasional differences of more than 5 K. The warm bias increased with height in the lower stratosphere. On the other hand, UKMO temperatures were also frequently found to be lower than radiosonde values. *Pullen and Jones* [1997] compared UKMO temperatures for the 1994/1995 Arctic winter to temperatures obtained independently from ozonesondes. They too found a positive bias in the UKMO temperatures, with values near the NAT existence threshold overestimated by almost 2 K at 475 K and 550 K. Significant scatter, increasing with altitude, was also found. *Manney et al.* ["Lower stratospheric temperature differences between meteorological analyses in two cold Arctic winters and their impact on polar processing studies", submitted, 2001 (hereinafter *Manney et al.*, submitted)] specifically compared several meteorological analyses during February 1996; UKMO minimum temperatures were frequently 1–2 K higher than those from most other analyses

Table 1. List of Parameters in Standard Model Runs

Parameter	Value
H_2O	5.0 ppmv
H_2SO_4	0.2 ppbv
HNO_3	MLS when T>205 K, or 10 ppbv
NAT number density	10^{-4} cm^{-3}
Refractive index	NAT: 1.6; LTA: variable[a]
Time Halfwidth[b]	12 hours
Latitude Halfwidth[b]	2°
Longitude Halfwidth[b]	7°

[a]The LTA refractive index is calculated using the values for binary H_2SO_4/H_2O solutions tabulated by *Palmer and Williams* [1975] (see text).

[b]The halfwidth values are used in the gridding procedure to obtain estimates of measured quantities at each timestep; thus they affect only the data estimates along the trajectory, not the PSC composition model results.

at 50 hPa, with slightly larger differences at 30 hPa. These studies suggest the degree of uncertainty in the UKMO temperatures that must be considered in interpreting our results. Since our application relies on temperature estimates along a trajectory, the temperature uncertainty is exacerbated by the lack of time resolution in the UKMO fields, which are available only once daily at 1200 UT. In addition, the errors accumulated in the trajectory calculations are poorly characterized and may be large. Temperatures along some of the trajectories shown here calculated based on several commonly-used meteorological analyses, including those from the UKMO, the U.S. National Centers for Environmental Prediction (NCEP) [*Gelman et al.*, 1994], and the NCEP/National Center for Atmospheric Research (NCAR) Reanalysis Project (REAN) [*Kalnay et al.*, 1996], occasionally differ by up to 10 K, with the largest differences occurring in warm regions. Although the variations between the meteorological analyses are considerably smaller (usually 3 K or less) in the low-temperature regions, they can still lead to substantial differences in model results. To explore the impact of the temperature uncertainty, we show results from model calculations made using both the reported UKMO temperature and a value reduced by 3 K (referred to as the "T–3 K" runs in the discussion below).

We have relied on an equilibrium model to characterize NAT formation. But NAT particles grow slowly [e.g., *Peter*, 1997, and references therein] and require a long duration at low temperatures to reach their full equilibrium size. In the Arctic, low temperatures are usually confined to relatively small regions that are not concentric with the vortex, so typical exposure times to PSC conditions are relatively short (less than a few days) [*Manney et al.*, submitted]. Thus opportunities for NAT particles to develop fully and deplete HNO_3 down to its equilibrium concentration are limited, and nonequilibrium mixtures of different cloud types are likely to be very common. If a PSC has not yet reached equilibrium at the time it is observed by MLS/POAM, then the measured HNO_3/extinction is expected to fall between the LTA and the equilibrium NAT model curves.

Usually a single data point contributes to the estimate at several successive timesteps, so the data do not reflect variations along the trajectory as rapidly as the models; this is particularly true for POAM. Taking into account the timescales over which many of the PSC formation and dissipation mechanisms are thought to act, a compromise was reached in selecting the temporal coincidence criterion (12 hours) to maximize data coverage along the orbit while minimizing the risk of sampling air measured under completely different conditions than those of the idealized parcels. Changing the time halfwidth used in the data gridding procedure changes the number of timesteps along the trajectory at which data estimates are available (and occasionally changes the estimated values themselves slightly). Similar caveats also apply to the spatial coincidence criteria.

By interpolating MLS and POAM data to a common trajectory for these comparisons, we have tried to ensure that

Table 2. List of Sensitivity Tests

Parameter Changed	New Value
H_2O	4.0 ppmv
H_2O	6.0 ppmv
H_2SO_4	0.5 ppbv
HNO_3[a]	various
NAT number density	0.001 cm^{-3}
NAT number density	0.01 cm^{-3}
NAT number density	0.1 cm^{-3}
NAT number density	1 cm^{-3}
NAT number density	10 cm^{-3}
LTA refractive index[a]	1.5% larger
Assumed UKMO Temperature Bias[b]	3.0 K
Assumed UKMO Temperature Bias[a,b]	1.0 K
Assumed UKMO Temperature Bias[a,b]	2.0 K
Assumed UKMO Temperature Bias[a,b]	6.0 K
Assumed UKMO Temperature Bias[a,b]	7.0 K
Assumed UKMO Temperature Bias[a,b]	8.0 K
Assumed UKMO Temperature Bias[a,b]	-0.5 K
Assumed UKMO Temperature Bias[a,b]	-1.0 K
Assumed UKMO Temperature Bias[a,b]	-2.0 K
Meteorological Analyses [a]	NCEP
Meteorological Analyses [a]	REAN
Time Halfwidth[c]	6 hours
Latitude Halfwidth[c]	1.0°
Longitude Halfwidth[c]	3.5°

[a]These tests only run for selected cases.

[b]This value is subtracted from the temperatures provided by the UKMO analyses to account for possible biases.

[c]Changes to these parameters affect only the data estimates along the trajectory, not the model results.

both instruments are sampling the same air. This may not necessarily be the case, however, if our coincidence criteria are too loose. Cloud composition may not be uniform over the distance separating the MLS and POAM observations. In a few cases, the MLS and POAM points, while still satisfying the coincidence criteria, may be sufficiently distant that the air parcels at those locations may have experienced slightly different temperature histories and thus may display a different character.

Some of the fluctuations seen in the MLS HNO_3 abundances may have arisen from "natural" (i.e., dynamical) variability inside the vortex and would therefore not be reproduced by any of the PSC composition models. A small degree of HNO_3 depletion without significant aerosol enhancement may also have arisen if particles falling from above scavenged some HNO_3 as they passed through a given atmospheric layer. Alternatively, sedimenting particles still resident in a given layer may contribute more observed aerosol extinction than can be accounted for by the observed gas-phase HNO_3 depletion.

Because extravortex air is generally characterized by lower HNO_3 abundances [e.g., *Santee et al.*, 1999, and references therein] and higher aerosol extinction values [e.g., *Kent et al.*, 1985; *Thomason and Poole*, 1993], entrainment of lower-latitude air into the vortex can produce a signature akin to that of PSC formation. Therefore, to properly assess the observed changes in HNO_3 and aerosol extinction and their relationships to the PSC composition models, in some cases it is necessary to consider the possibility of exchange of air between the polar vortex and midlatitudes. We evaluate the likelihood of cross-vortex horizontal transport and mixing with high-resolution PV maps from three-dimensional (3D) reverse-trajectory (RT) calculations [*Sutton et al.*, 1994; *Manney et al.*, 1998], which have been demonstrated [*Fairlie et al.*, 1997; *Manney et al.*, 2000] to be useful in refining the strong gradients in tracer fields across the vortex boundary. Space constraints prohibit showing these calculations, but they are mentioned in the discussion of individual cases where appropriate.

Finally, instrumental effects are most likely a significant factor. Clouds may be inhomogeneous on a scale smaller than that distinguishable in the satellite measurements. In addition, apparent inconsistencies in the MLS and POAM data sets may simply be a consequence of their different vertical resolutions: The HNO_3 at a particular level may actually reflect activity somewhere else in the $\sim$6 km plug of air that MLS senses, while POAM, with $\sim$1 km vertical resolution, sees nothing; conversely, a feature present in the POAM data may be too smeared out in the MLS data to be discernible. For example, vertical redistribution of HNO_3 through sedimentation and evaporation of PSC particles within the 6-km MLS sample volume could cause enhanced extinction at the POAM altitude but be imperceptible in the MLS measurements. This possibility is explored through various sample calculations and sensitivity tests for a number of cases.

4.3. Overview of Results

Trajectories were launched from all POAM occultation events that were both inside the vortex (PV $>$ 0.25×10^{-4} $\mathrm{K\,m^2\,kg^{-1}\,s^{-1}}$) and at a temperature below 200 K at 465 K during the 17 days in the MLS 1995/1996 late-winter north-looking observing period. Trajectories were also calculated for other warm-air and/or extravortex occultations if they registered a category "2" or "3" PSC detection (see section 2.2).

Of the 75 occultation events satisfying these criteria, 20 were situated on the edge of the vortex. The trajectories initialized from these locations skirted the vortex edge, and they were characterized by relatively warm temperature histories. HNO_3 abundances were fairly low and exhibited a large degree of scatter along the trajectory, and POAM measured relatively high aerosol extinction values. Because extravortex air is generally characterized by lower HNO_3 abundances [e.g., *Santee et al.*, 1999, and references therein] and higher aerosol extinction values [e.g., *Kent et al.*, 1985; *Thomason and Poole*, 1993], some vortex edge cases may be indicative of the intrusion of extravortex air and not PSC formation. In any event, separating the microphysical and dynamical effects would be extremely difficult even with a detailed modelling effort, and none of these cases are discussed further here.

In eight of the 75 cases the occultation terminated at an anomalously high altitude (usually 24–29 km, compared to the typical POAM minimum altitude of about 8.5 km [*Fromm et al.*, 1999]). For high Zmin cases, the altitude of the cloud top is believed to be 1–2 km below the occultation termination altitude [*Fromm et al.*, 1999]. Since the actual center altitude of the cloud is not known for these cases, it is difficult to make comparisons with model behavior. Although lower altitudes were usually very cold (e.g., at or below the frost point at 465 K), at the occultation termination altitude temperatures were generally not low, in some cases not below, or even near, PSC existence thresholds. Yet the cloud opacity was high enough to cause premature termination of the occultation. Interestingly, in a few of these cases the MLS HNO_3 abundances at the occultation termination altitude were also anomalous, much lower than at other points along the trajectory. Thus the aerosol extinction and HNO_3 fields appear to be more highly perturbed at the top of a strong (possibly water ice) PSC than would be expected based on local meteorological conditions. Comparisons at

465 K (rather than the occultation cutoff altitude) were not especially illuminating since temperatures along the trajectory dropped precipitously to the frost point, and all of the models and the MLS measurements exhibited a similar rapid decline in HNO_3. Therefore the high Zmin cases are not considered further in this study.

Three of the cases were characterized by both low HNO_3 and low extinction values; these will be discussed further in section 4.5. Twenty-three cases represented coincident measurements inside a cloud (i.e., with high extinction and low HNO_3 values), and 21 represented cloud-free air (i.e., with low extinction and high HNO_3 values). In most of the latter cases no PSCs were captured in either data set, because their trajectories passed through generally warm regions that did not experience cloud cycles or because data were missing along the trajectories during cloud activity. However, a few did reflect PSC activity at some point along their path, either before or after the initialization occultation event, with data available from one or both instruments. That is, even though at the time of the particular trajectory initialization no PSC was present, the air parcels at the occultation location still experienced PSC conditions on at least one other occasion as they journeyed around the vortex in the 5 days before or after the initialization time. We identified these sets of cases as the ones most likely to provide insight into PSC processes.

In general we found our approach of comparing both HNO_3 and aerosol extinction measurements to modelled quantities along air parcel trajectories to be very successful in capturing PSC formation, development, and dissipation phases. A strong correlation was found between low-temperature, low-HNO_3, and high-extinction points. Furthermore, the observed behavior along the Lagrangian paths was in most cases within the range predicted by equilibrium LTA and NAT models of PSC composition. Significantly, at no time along the trajectories (when there was data coverage) did the models display large changes in either HNO_3 abundances or aerosol extinction values that were not reflected in the data. We can thus state with confidence that these satellite HNO_3 and aerosol extinction data can be used to track PSC evolution along air parcel trajectories.

We enjoyed less success, however, in determining the specific types of PSCs that were forming. In general a large degree of overlap in the comparisons between the models and the data prevented conclusive identification of PSC composition or phase. While some examples were consistent with specific PSC formation mechanisms, no single set of assumptions allowed a majority of the cases to be explained. Many cases exhibited sufficient ambiguity that a variety of different formation scenarios could be invoked, especially with some judicious tweaking of model parameters. There were too many unmeasured quantities and too many large uncertainties in both measurements (including the meteorological analyses) and model calculations to allow conclusions about the exact composition of the PSCs in most of these cases to be formulated with a high degree of confidence.

Therefore, although we see evidence for the occurrence of LTA and possibly also for phase transitions between LTA and solid (NAT) PSCs, a rigorous accounting of the various processes observed is not practicable. We refrain here from attempting to compile from these data sets any overall statistics on PSC formation processes. We have, however, selected six of the most tantalizing cases to present in detail in the next two sections. These examples serve to illustrate both the promise and the perils of our Lagrangian approach to studying PSCs with satellite data.

4.4. Case Studies of PSC Composition

The initialization occultations for the six selected cases are identified on the maps in Plate 1, and additional pertinent information for each case is given in Table 3. Note that the selected cases are not presented in chronological order. The paths traced by the parcels along both the backward and forward trajectories are shown in Plate 2. In several cases the parcels traverse the same geographic region two or even three times over the course of the 10-day study period. Note also that these cases do not all depict separate PSC events. In reality only a few different PSCs have been sampled multiple times by these trajectories. The temperature histories, model calculations, and MLS HNO_3 and POAM aerosol extinction values along the combined 10-day trajectory are shown in Plate 3. The PSC activity illustrated by these cases may occur at any time along the trajectories, i.e., before, during, or after the initialization occultation events.

One of the most straightforward and least ambiguous examples is shown in case #1 (Plate 3a). The occultation in this case was made near the center of the region of depleted HNO_3 on 17 February (see Plate 1). Although the parcels experienced PSC conditions 4–5 days prior to the observation time, they subsequently underwent warming to above 210 K, near the sulfuric acid tetrahydrate (SAT) melting point [*Middlebrook et al.*, 1993; *Zhang et al.*, 1993]. Therefore, prior to the occultation time the HNO_3 had returned to the gas phase and the majority of the preexisting aerosols were probably in a liquid state. Temperatures then fell relatively rapidly, dipping below 190 K briefly around the initialization point before rising again; the total duration of temperatures below the NAT existence threshold was about 1.5 days. The MLS HNO_3 data are matched best by the LTA model throughout most of the PSC episode, although near the end of the cloud cycle the depletion suggested by the MLS data is larger than that predicted by the LTA model, possibly indicating the

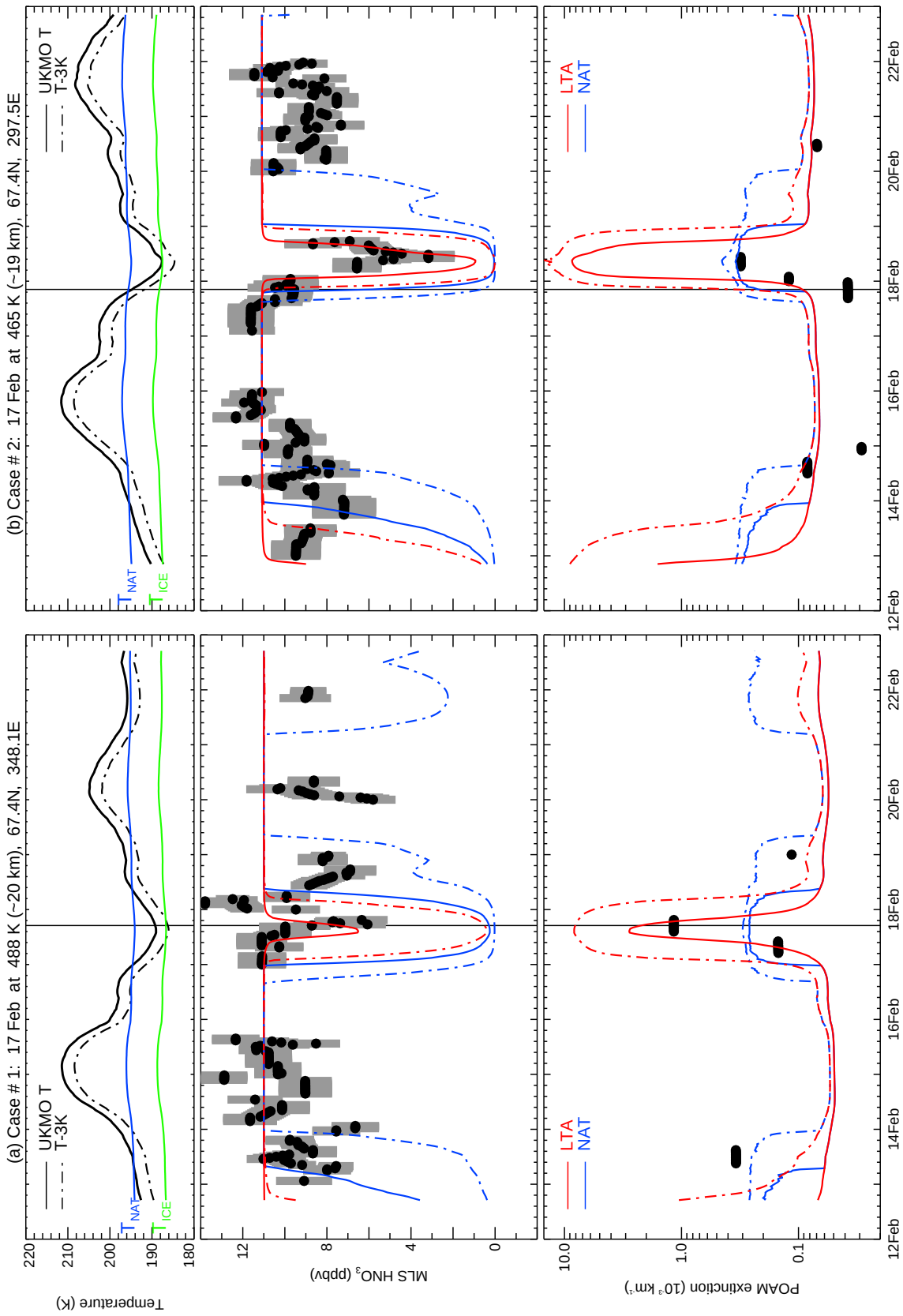

Plate 3. Measurements and model results along the trajectories for each of the 6 selected cases (see text). The date, location, potential temperature, and corresponding approximate altitude at which both the backward and forward trajectories are initialized are specified for each case. The thin vertical line bisecting the plots indicates the time of the initialization point. The top panel shows the temperature evolution, with the solid black line representing the temperatures from the UKMO analyses and the dash-dot black line representing values 3 K lower than the reported ones at each timestep (to account for a possible high bias in the UKMO analyzed temperatures). Also shown in this panel are the NAT (blue line) and water ice (green line) formation thresholds. The other two panels compare measured and modelled gas-phase HNO_3 (middle) and aerosol extinction (bottom). The standard model runs (solid lines) are based on the reported UKMO temperatures; tests are also run with the temperature reduced by 3 K everywhere along the trajectory (dash-dots lines). Results from equilibrium LTA (red lines) and NAT (blue lines) composition models are shown. Table 1 lists the values of the various parameters in the standard model runs. A gridding procedure (see text for details) is applied to obtain estimates of MLS HNO_3 (middle panel) and POAM aerosol extinction (bottom panel) at each timestep (black dots, with the estimated error bars shaded in grey).

Table 3. List of Case Study Initialization Occultations

Case	Date (1996)	POAM Occultation #	PSC Altitude	Initial level	Lat	Lon
1	17 Feb	12414	21 km	488 K	67.4°N	348.1°E
2	17 Feb	12416	–	465 K	67.4°N	297.5°E
3	3 Mar	12627	19 km	438 K	67.7°N	359.8°E
4	13 Feb	12356	20 km	466 K	67.2°N	15.5°E
5	13 Feb	12355	20 km	478 K	67.2°N	40.8°E
6	17 Feb	12411	18 km	433 K	67.4°N	64.0°E

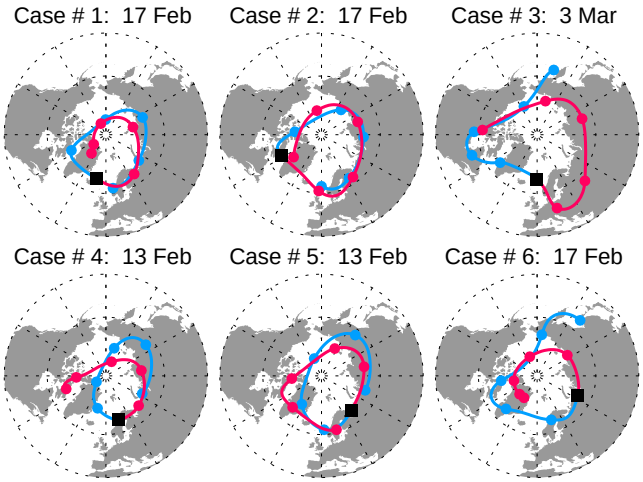

Plate 2. Backward (blue) and forward (red) trajectory paths from the initialization occultation (black squares) for the 6 selected cases (see text). The occultations are identified on the maps in Plate 1, and additional information for each case is given in Table 3. Colored dots represent the parcel positions every 24 hours along the trajectory.

presence of mixed (solid and liquid) clouds. The POAM extinction data are also in excellent agreement with liquid or mostly-liquid clouds.

The occultation in case #2 (Plate 3b) was made upstream from that in case #1 in air that was cloud-free at the time of observation (see Plate 1). Although the parcels in these two cases passed through essentially the same area of PSC activity, case #2 presents a much more ambiguous picture. Again, the MLS HNO_3 data are matched best by the LTA model. Measured and modelled HNO_3 concentrations agree well during the HNO_3 recovery portion of the cloud cycle, but initially the LTA model predicts more HNO_3 uptake than is observed. This apparent lag between the observed and predicted decrease in gas-phase HNO_3 is not resolved by altering the coincidence criteria used to interpolate the data along the trajectory (not shown) or other model parameters (e.g., H_2O or H_2SO_4 mixing ratios; not shown). Furthermore, the LTA model significantly overestimates the extinction measured by POAM, which agrees well with the NAT equilibrium curve. Thus no single PSC composition model can be made to match the two sets of measurements.

Case #3 (Plate 3c) depicts the opposite situation, in which the two data sets in combination allow a more definitive determination to be made than would either one alone. The scatter in the HNO_3 concentrations and the slightly elevated aerosol extinction values along the back trajectory suggest entrainment of lower latitude air as the parcels passed near the vortex edge in the days leading up to the PSC event. This supposition is supported by high-resolution 3D RT calculations, which indicate interleaved wisps of high and low PV air in these regions at this time (not shown). The parcels then underwent fairly rapid synoptic cooling, reaching a minimum temperature of 193 K. *Santee et al.* [1996] investigated the low-HNO_3 pocket on March 3 and showed results from high-resolution 3D transport calculations that rule out any influence of lower-latitude air on the HNO_3 val-

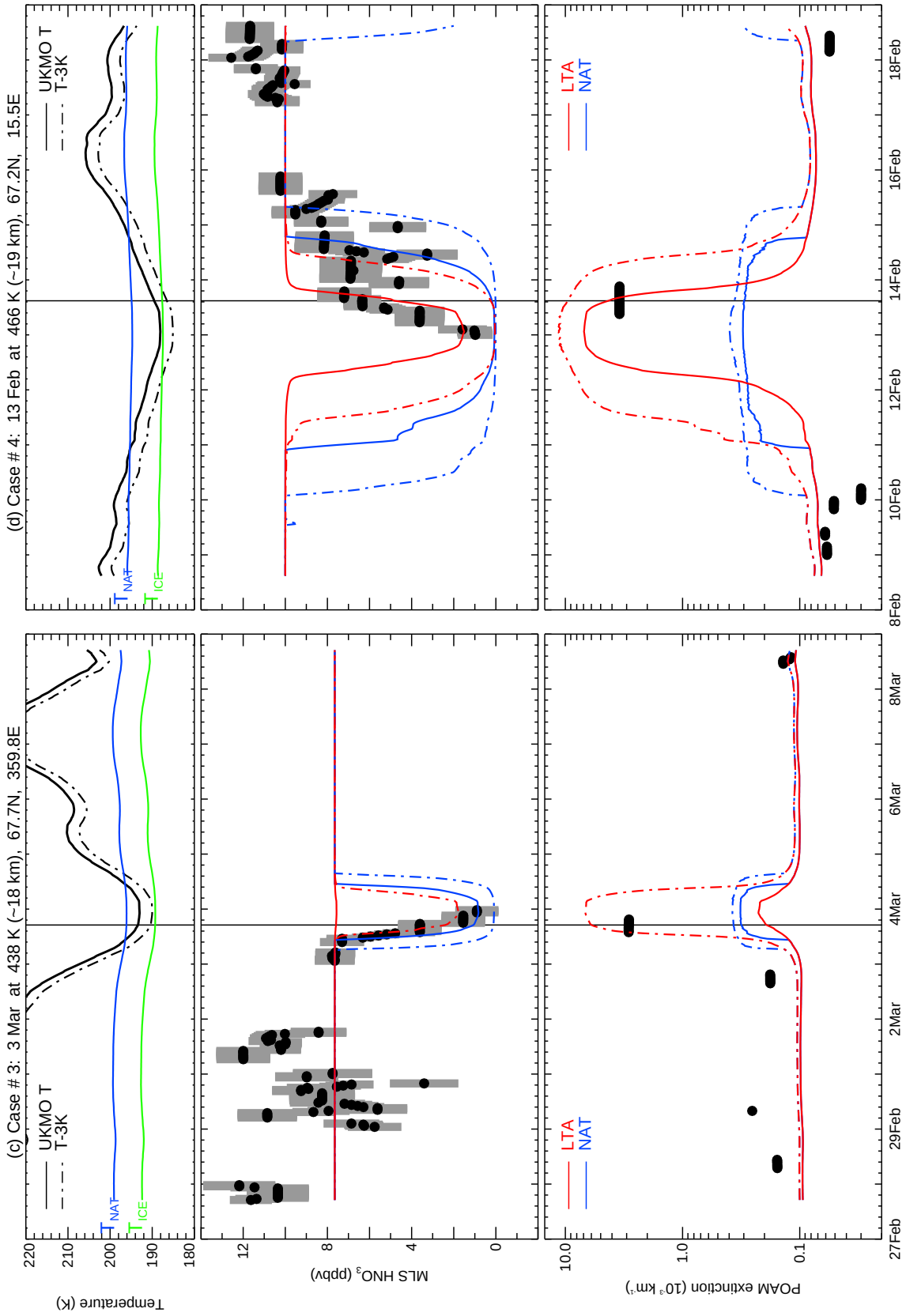

Plate 3. Continued.

ues in this region. HALOE onboard UARS also measured aerosol extinctions indicative of PSCs on March 3 and 4 [*Hervig*, 1999], although the latitude of the HALOE occultations was considerably lower (52°N) than that of POAM (67°N). Therefore, despite the earlier behavior, the observed HNO_3 decrease at the initialization time is associated with PSC activity. Although the MLS data fall along the equilibrium NAT model curve for uncorrected UKMO temperatures from the very start of HNO_3 depletion, it is unlikely that a fully-developed NAT cloud would appear without a prior LTA stage experiencing low temperatures for a longer period of time [e.g., *Peter*, 1997; *Tabazadeh et al.*, 2001]. In addition, a very high (0.2 cm^{-3}; not shown) number density of NAT particles would be required to match the POAM extinction. On the other hand, both MLS and POAM data are in excellent agreement with the LTA model when the temperatures are reduced by 3 K. Thus the most probable explanation for this case is a cloud composed of a majority of liquid particles, under the assumption of a 3 K high bias in the UKMO temperatures at this time.

In contrast to the previous cases, in case #4 (Plate 3d) temperatures along the trajectory had been below the NAT threshold for almost 3 days prior to the occultation on February 13. In the latter half of the cloud cycle, despite the prolonged exposure to low temperatures, the MLS data match the LTA model closely, indicating far less depletion than that predicted by the equilibrium NAT model. The POAM data are also in excellent agreement with LTA. After the initialization time, the MLS data depart from the LTA behavior and show depletions between those of the LTA and equilibrium NAT models. This pattern is robust even when other values for the H_2O mixing ratio or gridding coincidence criteria are used (not shown). Thus the number of solid particles may have been increasing by this time. On the other hand, immediately preceding the initialization time, the parcels travelled through an area of extreme cold near Iceland in which POAM recorded a high Zmin event, indicating the presence of water ice clouds [*Fromm et al.*, 1999] (compare Plates 1 and 2). An alternative explanation for this case is that both instruments may have captured the transition between a water ice PSC and cloud-free conditions.

Case #5 (Plate 3e) is situated just downstream from case #4 (see Plate 1). Although the parcels in the two cases traversed the same general vicinity and were exposed to low temperatures for similarly prolonged periods, the minimum temperatures attained in case #5 ($\sim$191 K) were not as low. Unfortunately, MLS missed all but the tail end of this PSC episode, but POAM observed the cloud both in the middle and at the edge. By the initialization point, temperatures had risen to the NAT existence threshold after spending almost 2.5 days below it. While the measured extinction agrees well with the LTA model in the middle of the low-temperature region, it exceeds that predicted by the models at the initialization point. Even for a T–3 K model run with a H_2O mixing ratio of 6 ppmv (not shown), the measured extinction at the initialization time still slightly exceeds the predicted LTA value. Nor does the standard NAT model provide results that fit the POAM data. If, however, a number density of nucleated particles of 0.1 cm^{-3} is used (not shown), then the measured extinction at the initialization time matches the equilibrium NAT model for the reported UKMO temperatures. Thus our results may signify conversion from LTA to NAT particles in the period between the two POAM measurements.

For our final example we show another case that, while interesting, is difficult to reconcile with PSC models. Along the back trajectory, case #6 (Plate 3f) samples a slightly different portion of the same general PSC region in the vicinity of Iceland that was observed at the initialization time in case #1 and along the forward trajectory in case #2 (see Plates 1 and 2). Temperatures along the trajectory were relatively high until February 15, so the background aerosols are expected to have been liquid. Temperatures reached their minimum (just below 192 K) on February 16; by the initialization time they had been below the NAT existence threshold for 2 full days. As in case #3, the MLS data seem to imply immediate NAT formation, although the observed HNO_3 starts to decrease when UKMO temperatures are still $\sim$200 K. Since we consider the direct formation of NAT to be unlikely, a more probable diagnosis for this case is initial LTA formation under the assumption that the UKMO temperatures are in error by 3 K at this point along the trajectory. However, the POAM extinction data halfway through the cloud event are consistent only with the LTA model calculated using the UKMO temperatures as reported. This does not necessarily represent a conflict, since there is no reason to expect that temperatures are biased high uniformly at every point along the trajectory. Toward the end of the episode the MLS HNO_3 matches the NAT equilibrium model very closely, but, for the standard run, the POAM extinction does not. If, however, a number density of 0.01 cm^{-3} is employed instead, then the mid-PSC POAM point is still matched best by the LTA curve, while the extinction during PSC dissipation agrees extremely well with the NAT model calculated for the reported UKMO temperatures (not shown). This case could, therefore, be interpreted as suggesting observation of a phase transition between LTA and NAT by both instruments. Several other sensitivity tests were performed to evaluate alternative explanations, but none produced a consistent picture satisfying both data sets.

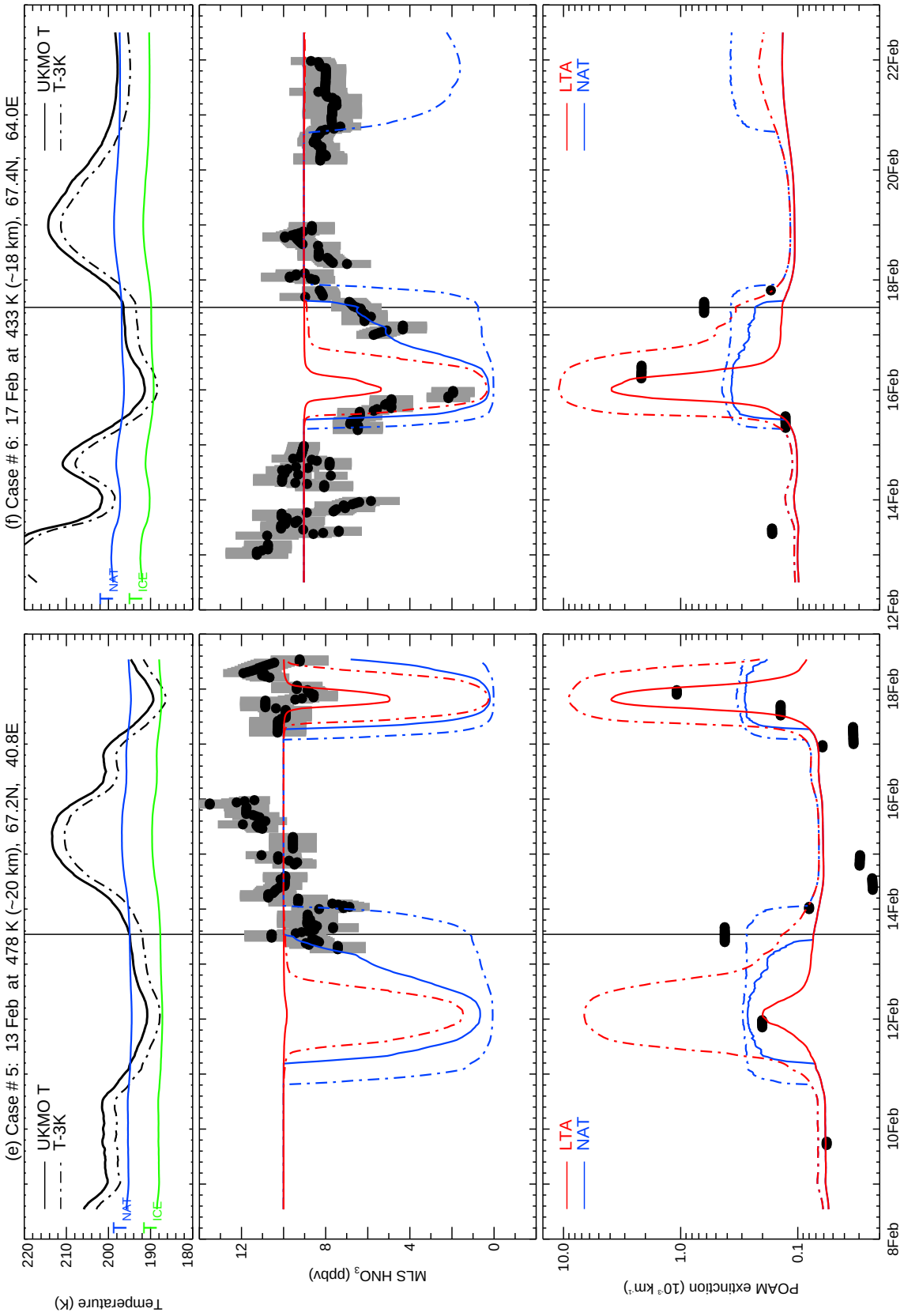

Plate 3. Continued.

4.5. Case Studies of Denitrification

In the majority of cases in which both PSC formation and dissipation were observed, HNO_3 concentrations eventually rebounded to their pre-PSC values after the parcels exited the cold region. Full recovery in gas-phase HNO_3 following PSC activity implies that no denitrification has taken place on a scale comparable to the MLS sample volume. Of course, MLS is not sensitive to localized redistribution of HNO_3 within the 6-km layer corresponding to its vertical resolution. Denitrification appears to have been minimal even when solid particles may have formed, e.g., in case #6. In other cases full recovery also appears likely (e.g., #4 and #5), but lack of HNO_3 measurements prior to PSC formation precludes definitive assessment.

Two cases in which the HNO_3 does not appear to recover fully are #1 and #2. MLS measurements on February 20–21 indicate residually low HNO_3 abundances downstream from the PSC. Halving the temporal and spatial halfwidths in the gridding procedure (see section 4.1) reduces the number of timesteps for which data estimates are available but does not eliminate the points with low HNO_3 downstream from the PSC. In case #2 the POAM measurement on February 20 indicates background levels of aerosol extinction, and high-resolution 3D RT calculations provide no evidence of intrusion of extravortex air. Thus the February 20–21 observations suggest denitrification of roughly 20% ($\sim$2 ppbv) over the 6-km stratum of air sampled by MLS. From the POAM measurements, however, the thickness of the PSC is estimated to be $\sim$3 km, implying a lower limit of about 40% denitrification, assuming that the HNO_3 was removed throughout the entire 3-km cloud layer. On the other hand, the inference of denitrification from these cases is at odds with the cloud compositions discussed in section 4.4. Although in case #2 the POAM measurement in the middle of the cloud may indicate the presence of solid particles, the MLS data are matched well by the LTA model. Case #1 also appears to be consistent with an LTA phase. LTA PSCs are composed of relatively small droplets that are not subject to significant gravitational settling [e.g., *Tabazadeh et al.*, 1994a]. In addition, the total amount of available HNO_3 is set to about 11 ppbv in these cases, based on the last point along the back trajectory for which the temperature is above 205 K (see section 4.1). Setting the total HNO_3 amount to 10 ppbv instead (not shown) results in very little change to the model comparisons during the PSC event but reduces the discrepancy between measured and modelled HNO_3 values on February 20–21 to within the measurement error bars for most (but not all) of the points. Therefore, although suggestive of denitrification, these cases do not offer incontrovertible proof.

Three occultations characterized by both low extinction and low HNO_3 values, mentioned in section 4.3, may also suggest some denitrification. In these cases (not shown), MLS records a significant dip in HNO_3 in a series of points before the occultation, but POAM does not detect significant aerosol enhancement. In all three cases, the RT calculations show that air from the vicinity of previous strong PSC events has been advected to the occultation location by the time of the measurements. Prongs of air denitrified during an earlier PSC episode could influence the HNO_3 values along this trajectory, while leaving the extinction values unaffected. However, in two of the cases the RT calculations also suggest that large intrusions of lower-latitude air enter the vortex at or near the occultation site. In addition, the NAT model predicts a slight amount of HNO_3 sequestration if the UKMO temperatures are reduced by 3 K (although the depletion pattern in the model curve does not conform exactly to the observed decrease in HNO_3). Although either entrainment of extravortex air or PSC growth should produce a signature in the aerosol extinction, these processes cannot be completely ruled out, and once again a conclusive finding of denitrification cannot be made.

Thus, although we see inconclusive hints that denitrification has occurred in a few of the cases, the majority indicate that gas-phase HNO_3 fully recovers to pre-PSC abundances following cloud evaporation, even when there is some indication that solid particles may have formed. During the late 1980s and the 1990s, many of the northern winters were exceptionally cold [*Zurek et al.*, 1996; *Pawson and Naujokat*, 1999; *Manney and Sabutis*, 2000], and patches of partially denitrified air were observed on several occasions [*Arnold et al.*, 1989, 1998; *Fahey et al.*, 1990, 2001; *Rex et al.*, 1999; *Kondo et al.*, 1999, 2000]. In particular, based on ER–2 aircraft measurements made at the edge of the Arctic polar vortex on February 1, 1996, *Hintsa et al.* [1998] deduced denitrification of more than 50% in the layer between 18 and 19 km ($\sim$450–465 K). While this is a substantial amount of denitrification, it is very limited in vertical extent. The vertical resolution of the MLS measurements is too coarse to allow such narrow layers to be distinguished. *Dessler et al.* [1999] also analyzed MLS HNO_3 measurements for several Arctic winters in the early 1990s and similarly found the degree of denitrification to be limited. Only during the 1999/2000 winter, when the area of temperatures less than 195 K was both unusually large and unusually persistent [*Manney and Sabutis*, 2000], did denitrification significant enough to be detected by MLS ($\sim$20%) occur over a sizeable fraction of the Arctic vortex (at equivalent latitudes of 70°N and higher) [*Santee et al.*, 2000]. Modelling studies by *Tabazadeh et al.* [2001] suggest that a larger vertical extent of the denitrified layers in 1999/2000, compared to other Arctic winters, facilitated their detection by MLS. We con-

clude that, although severe denitrification (50% or greater) may have occurred in highly localized regions in the Arctic in 1996, it did not occur over spatial scales comparable to or larger than the MLS field of view, even though it was a relatively cold winter when solid PSC particles may have been present over large areas for several days.

5. Summary and Conclusions

Our main goal in this study was to assess the viability of diagnosing PSC composition and denitrification using existing satellite measurements. We correlated UARS MLS measurements of gas-phase HNO_3 with POAM II measurements of aerosol extinction during the northern hemisphere late winter of 1995/1996. A Lagrangian approach was used to track the entire cloud cycle from formation through dissipation. Air parcel trajectories were calculated both forward and backward from the locations of POAM occultations, and the MLS and POAM data were interpolated to the parcel positions along the trajectory before, during, and after a PSC episode. The observed behavior of both HNO_3 and aerosol extinction was then compared to that predicted by LTA and NAT equilibrium composition models. Many sensitivity tests were run in an effort to evaluate the impact of the numerous uncertainties on our interpretations.

Extracting detailed quantitative information about the composition of individual PSCs by combining these satellite HNO_3 and aerosol data sets is a very difficult task. We found that, although these measurements can be used to track PSC evolution along air parcel trajectories, they are less successful in determining the composition or phase of the PSCs that are forming. In general there is a large degree of overlap in the comparisons between the models and the data. Although some examples are consistent with specific PSC formation mechanisms, no single set of model assumptions allows a majority of the cases to be explained. In addition to large uncertainties in both measurements (including the meteorological analyses) and model calculations, other factors that hampered interpretation of these cases include lack of colocated HNO_3, aerosol extinction, H_2O, and temperature measurements, and low horizontal and (for MLS) vertical resolution of the data.

Many of these deficiencies will be ameliorated in the upcoming Earth Observing System (EOS) Aura mission (see http://eos-aura.gsfc.nasa.gov). An enhanced version of the MLS instrument [*Waters*, 1999] will provide measurements with much better measurement coverage and vertical and horizontal resolution. EOS MLS will perform measurements with the instrument fields of view scanning the limb in the orbit plane to provide latitudinal coverage that will extend from 82°N to 82°S on every orbit, affording continuous monitoring of the polar regions (no monthly gaps as on UARS). The along-track separation between adjacent limb scans will be 165 km (as opposed to 500 km for UARS MLS), but the longitudinal separation between orbit tracks will be the same as it was for UARS MLS (e.g., ∼2600 km at the equator, ∼500 km at 70°N). The horizontal resolution will be ∼200–300 km along the line of sight and ∼10 km perpendicular to the line of sight (∼400 km×200 km for UARS MLS), and the vertical resolution of the retrieved products will be ∼3 km (∼6 km for UARS MLS). In addition to HNO_3, which will be measured with a single-profile precision of ∼2 ppbv (about the same as for UARS MLS), EOS MLS will obtain simultaneous measurements of H_2O and temperature with precisions of ∼0.2 ppmv and ∼0.5 K, respectively, in the lower stratosphere.

Other instruments on EOS Aura will also provide stratospheric measurements crucial to studies of PSC formation. In addition to simultaneous measurements of HNO_3, H_2O, and temperature, the High Resolution Dynamics Limb Sounder (HIRDLS) will obtain measurements of aerosol extinction. Expected precisions are 0.4 K for temperature and 1–5% for the HNO_3, H_2O, and aerosol extinction measurements. For the nominal observing mode, the profile spacing will 400–500 km along the line of sight; because the field of view is stepped in azimuth several times during a nominal scan, the horizontal spacing across the orbit track will also be 400–500 km. Measurement resolution will be 250–300 km along the line of sight and ∼10 km perpendicular to it, and the vertical field of view will be 1 km. HIRDLS will thus provide observations with horizontal and vertical resolution unprecedented in a global data set. The Tropospheric Emission Spectrometer (TES) will also measure HNO_3, H_2O, and temperature in the stratosphere in the limb mode, with vertical resolution of 2.5–3.5 km, horizontal resolution of 23 km (cross-track) by 120 km (along-track), and errors of less than 10% for atmospheric constituents and 1 K for temperature.

Acknowledgments. We are grateful to our MLS colleagues, particularly N. Livesey and L. Froidevaux, for their efforts in producing the MLS version 5 retrievals. We thank the U.K. Met Office (especially R. Swinbank) for meteorological analyses. The valuable comments of the two anonymous referees are appreciated. Work at the Jet Propulsion Laboratory, California Institute of Technology, was done under contract with the National Aeronautics and Space Administration.

References

Arnold, F., H. Schlager, J. Hoffman, P. Metzinger, and S. Spreng, Evidence for stratospheric nitric acid condensation from balloon and rocket measurements in the Arctic, *Nature*, *342*, 493–497, 1989.

Arnold, F., V. Bürger, K. Gollinger, M. Roncossek, J. Schneider,

and S. Spreng, Observations of nitric acid perturbations in the winter Arctic stratosphere: Evidence for PSC sedimentation, *J. Atmos. Chem.*, *30*, 49–59, 1998.

Barath, F. T., et al., The Upper Atmosphere Research Satellite Microwave Limb Sounder Instrument, *J. Geophys. Res.*, *98*, 10,751–10,762, 1993.

Beyerle, G., B. Luo, R. Neuber, T. Peter, and I. S. McDermid, Temperature dependence of ternary solution particle volumes as observed by lidar in the Arctic stratosphere during winter 1992/1993, *J. Geophys. Res.*, *102*, 3603–3609, 1997.

Brogniez, C., et al., Second European Stratospheric Arctic and Midlatitude Experiment campaign: Correlative measurements of aerosol in the northern polar atmosphere, *J. Geophys. Res.*, *102*, 1489–1494, 1997.

Carslaw, K. S., T. Peter, and S. L. Clegg, Modeling the composition of liquid stratospheric aerosols, *Rev. Geophys.*, *35*, 125–154, 1997.

Carslaw, K. S., et al., Particle microphysics and chemistry in remotely observed mountain polar stratospheric clouds, *J. Geophys. Res.*, *103*, 5785–5796, 1998.

Danilin, M. Y., M. L. Santee, J. M. Rodriguez, M. K. W. Ko, J. L. Mergenthaler, J. B. Kumer, A. Tabazadeh, and N. Livesey, Trajectory hunting: A case study of rapid chlorine activation in December 1992 as seen by UARS, *J. Geophys. Res.*, *105*, 4003–4018, 2000.

Deshler, T., and S. J. Oltmans, Vertical profiles of volcanic aerosol and polar stratospheric clouds above Kiruna, Sweden: Winters 1993 and 1995, *J. Atmos. Chem.*, *30*, 11–23, 1998.

Dessler, A. E., J. Wu, M. L. Santee, and M. R. Schoeberl, Satellite observations of temporary and irreversible denitrification, *J. Geophys. Res.*, *104*, 13,993–14,002, 1999.

Dye, J. E., D. Baumgardner, B. W. Gandrud, S. R. Kawa, K. K. Kelly, M. Loewenstein, G. V. Ferry, K. R. Chan, and B. L. Gary, Particle size distributions in Arctic polar stratospheric clouds, growth and freezing of sulfuric acid droplets, and implications for cloud formation, *J. Geophys. Res.*, *97*, 8015–8034, 1992.

Fahey, D. W., S. Solomon, S. R. Kawa, M. Loewenstein, J. R. Podolske, S. E. Strahan, and K. R. Chan, A diagnostic for denitrification in the winter polar stratospheres, *Nature*, *345*, 698–702, 1990.

Fahey, D. W., et al., The detection of large HNO_3-containing particles in the winter Arctic stratosphere, *Science*, *291*, 1026–1031, 2001.

Fairlie, T. D. A., R. B. Pierce, W. L. Grose, G. Lingenfelser, M. Loewenstein, and J. R. Podolske, Lagrangian forecasting during ASHOE/MAESA: Analysis of predictive skill for analyzed and reverse-domain-filled potential vorticity, *J. Geophys. Res.*, *102*, 13,169–13182, 1997.

Fromm, M. D., J. D. Lumpe, R. M. Bevilacqua, E. P. Shettle, J. Hornstein, S. T. Massie, and K. H. Fricke, Observations of Antarctic polar stratospheric clouds by POAM II: 1994–1996, *J. Geophys. Res.*, *102*, 23,659–23,672, 1997.

Fromm, M. D., R. M. Bevilacqua, J. Hornstein, E. P. Shettle, K. Hoppel, and J. D. Lumpe, An analysis of Polar Ozone and Aerosol Measurement POAM II Arctic stratospheric cloud observations, 1993–1996, *J. Geophys. Res.*, *104*, 24,341–24,357, 1999.

Gelman, M. E., A. J. Miller, R. M. Nagatani, and C. S. Long, Use of UARS data in the NOAA stratospheric monitoring program, *Adv. Space Res.*, *14*, 21–31, 1994.

Glaccum, W., , et al., The Polar Ozone and Aerosol Measurement instrument, *J. Geophys. Res.*, *101*, 14,479–14,487, 1996.

Hanson, D., and K. Mauersberger, Laboratory studies of the nitric acid trihydrate: Implications for the south polar stratosphere, *Geophys. Res. Lett.*, *15*, 855–858, 1988.

Hervig, M. E., Stratospheric clouds over England, *Geophys. Res. Lett.*, *26*, 1137–1140, 1999.

Hervig, M. E., K. S. Carslaw, T. Peter, T. Deshler, L. L. Gordley, G. Redaelli, U. Biermann, and J. M. Russell III, Polar stratospheric clouds due to vapor enhancement: HALOE observations of the Antarctic vortex in 1993, *J. Geophys. Res.*, *102*, 28,185–28,193, 1997.

Hintsa, E. J., et al., Dehydration and denitrification in the Arctic polar vortex during the 1995-1996 winter, *Geophys. Res. Lett.*, *25*, 501–504, 1998.

Kalnay, E., et al., The NCAR/NCEP 40-year reanalysis project, *Bull. Am. Meteorol. Soc.*, *77*, 437–471, 1996.

Kelly, K. K., A. F. Tuck, L. E. Heidt, M. Loewenstein, J. R. Podolske, S. E. Strahan, and J. F. Vedder, A comparison of ER-2 measurements of stratospheric water vapor between the 1987 Antarctic and 1989 Arctic airborne missions, *Geophys. Res. Lett.*, *17*, 465–468, 1990.

Kent, G. S., C. R. Trepte, U. O. Farrukh, and M. P. McCormick, Variation in the stratospheric aerosol associated with the north cyclonic polar vortex as measured by the SAM II satellite sensor, *J. Atmos. Sci.*, *42*, 1536–1551, 1985.

Kondo, Y., H. Irie, M. Koike, and G. E. Bodeker, Denitrification and nitrification in the Arctic stratosphere during the winter of 1996–1997, *Geophys. Res. Lett.*, *27*, 337–340, 2000.

Kondo, Y., et al., NO_y-N_2O correlation observed inside the Arctic vortex in February 1997: Dynamical and chemical effects, *J. Geophys. Res.*, *104*, 8215–8224, 1999.

Lumpe, J. D., et al., POAM II retrieval algorithm and error analysis, *J. Geophys. Res.*, *102*, 23,593–23,614, 1997.

Luo, B., U. K. Krieger, and T. Peter, Densities and refractive indices of $H_2SO_4/HNO_3/H_2O$ solutions to stratospheric temperatures, *Geophys. Res. Lett.*, *23*, 3707–3710, 1996.

Manney, G. L., and J. L. Sabutis, Development of the polar vortex in the 1999–2000 Arctic winter stratosphere, *Geophys. Res. Lett.*, *27*, 2589–2592, 2000.

Manney, G. L., R. W. Zurek, A. O'Neill, and R. Swinbank, On the motion of air through the stratospheric polar vortex, *J. Atmos. Sci.*, *51*, 2973–2994, 1994.

Manney, G. L., M. L. Santee, L. Froidevaux, J. W. Waters, and R. W. Zurek, Polar vortex conditions during the 1995–96 Arctic winter: Meteorology and MLS ozone, *Geophys. Res. Lett.*, *23*, 3203–3206, 1996a.

Manney, G. L., R. Swinbank, S. T. Massie, M. E. Gelman, A. J. Miller, R. Nagatani, A. O'Neill, and R. W. Zurek, Comparison of U.K. Meteorological Office and U.S. National Meteorological Center stratospheric analyses during northern and southern winter, *J. Geophys. Res.*, *101*, 10,311–10,334, 1996b.

Manney, G. L., J. C. Bird, D. P. Donovan, T. J. Duck, J. A. Whiteway, S. R. Pal, and A. I. Carswell, Modeling ozone laminae

in ground-based Arctic wintertime observations using trajectory calculations and satellite data, *J. Geophys. Res.*, *103*, 5797–5814, 1998.

Manney, G. L., H. A. Michelsen, F. W. Irion, G. C. Toon, M. R. Gunson, and A. E. Roche, Lamination and polar vortex development in fall from ATMOS long-lived trace gases observed during November 1994, *J. Geophys. Res.*, *105*, 29,023–29,038, 2000.

Middlebrook, A. M., L. T. Iraci, L. S. McNeill, B. G. Koehler, M. A. Wilson, O. W. Saastad, and M. A. Tolbert, Fourier transform-infrared studies of thin H_2SO_4/H_2O films: Formation, water uptake, and solid-liquid phase changes, *J. Geophys. Res.*, *98*, 20,473–20,481, 1993.

Naujokat, B., and S. Pawson, The cold stratospheric winters 1994/1995 and 1995/1996, *Geophys. Res. Lett.*, *23*, 3703–3706, 1996.

Nedoluha, G. E., R. M. Bevilacqua, K. W. Hoppel, M. Daehler, E. P. Shettle, J. H. Hornstein, M. D. Fromm, J. D. Lumpe, and J. E. Rosenfield, POAM III measurements of dehydration in the Antarctic lower stratosphere, *Geophys. Res. Lett.*, *27*, 1683–1686, 2000.

Ovarlez, J., and H. Ovarlez, Stratospheric water vapor content evolution during EASOE, *Geophys. Res. Lett.*, *21*, 1235–1238, 1994.

Palmer, K. F., and D. Williams, Optical constants of sulfuric acid: Application to the clouds of Venus?, *Appl. Opt.*, *14*, 208–219, 1975.

Pawson, S., and B. Naujokat, The cold winters of the middle 1990s in the northern lower stratosphere, *J. Geophys. Res.*, *104*, 14,209–14,222, 1999.

Peter, T., Microphysics and heterogeneous chemistry of polar stratospheric clouds, *Annu. Rev. Phys. Chem.*, *48*, 785–822, 1997.

Pullen, S., and R. L. Jones, Accuracy of temperatures from UKMO analyses of 1994/95 in the arctic winter stratosphere, *Geophys. Res. Lett.*, *24*, 845–848, 1997.

Randall, C. E., R. M. Bevilacqua, J. D. Lumpe, K. W. Hoppel, D. W. Rusch, and E. P. Shettle, Comparison of Polar Ozone and Aerosol Measurement (POAM) II and Stratospheric Aerosol and Gas Experiment (SAGE) II aerosol measurements from 1994 to 1996, *J. Geophys. Res.*, *105*, 3929–3942, 2000.

Randall, C. E., et al., An overview of POAM II aerosol measurements at 1.06 μm, *Geophys. Res. Lett.*, *23*, 3195–3198, 1996.

Rex, M., et al., In situ measurements of stratospheric ozone depletion rates in the Arctic winter of 1991/1992: A Lagrangian approach, *J. Geophys. Res.*, *103*, 5843–5853, 1998.

Rex, M., et al., Subsidence, mixing, and denitrification of Arctic polar vortex air measured during POLARIS, *J. Geophys. Res.*, *104*, 26,611–26,623, 1999.

Santee, M. L., G. L. Manney, W. G. Read, L. Froidevaux, and J. W. Waters, Polar vortex conditions during the 1995–96 Arctic winter: MLS ClO and HNO_3, *Geophys. Res. Lett.*, *23*, 3207–3210, 1996.

Santee, M. L., A. Tabazadeh, G. L. Manney, R. J. Salawitch, L. Froidevaux, W. G. Read, and J. W. Waters, UARS MLS HNO_3 observations: Implications for Antarctic polar stratospheric clouds, *J. Geophys. Res.*, *103*, 13,285–13,314, 1998.

Santee, M. L., G. L. Manney, L. Froidevaux, W. G. Read, and J. W. Waters, Six years of UARS Microwave Limb Sounder HNO_3 observations: Seasonal, interhemispheric, and interannual variations in the lower stratosphere, *J. Geophys. Res.*, *104*, 8225–8246, 1999.

Santee, M. L., G. L. Manney, N. J. Livesey, and J. W. Waters, UARS Microwave Limb Sounder observations of denitrification and ozone loss in the 2000 Arctic late winter, *Geophys. Res. Lett.*, *27*, 3213–3216, 2000.

Steele, H. M., K. Drdla, R. P. Turco, J. D. Lumpe, and R. M. Bevilacqua, Tracking polar stratospheric cloud development with POAM II and a microphysical model, *Geophys. Res. Lett.*, *26*, 287–290, 1999.

Sutton, R. T., H. MacLean, R. Swinbank, A. O'Neill, and F. W. Taylor, High-resolution stratospheric tracer fields estimated from satellite observations using Lagrangian trajectory calculations, *J. Atmos. Sci.*, *51*, 2995–3005, 1994.

Swinbank, R., and A. O'Neill, A stratosphere-troposphere data assimilation system, *Mon. Weather Rev.*, *122*, 686–702, 1994.

Tabazadeh, A., R. P. Turco, K. Drdla, M. Z. Jacobson, and O. B. Toon, A study of Type I polar stratospheric cloud formation, *Geophys. Res. Lett.*, *21*, 1619–1622, 1994a.

Tabazadeh, A., R. P. Turco, and M. Z. Jacobson, A model for studying the composition and chemical effects of stratospheric aerosols, *J. Geophys. Res.*, *99*, 12,897–12,914, 1994b.

Tabazadeh, A., M. L. Santee, M. Y. Danilin, H. C. Pumphrey, P. A. Newman, P. J. Hamill, and J. L. Mergenthaler, Quantifying denitrification and its effect on ozone recovery, *Science*, *288*, 1407–1411, 2000.

Tabazadeh, A., E. J. Jensen, O. B. Toon, K. Drdla, and M. R. Schoeberl, Role of the stratospheric polar freezing belt in denitrification, *Science*, *291*, 2591–2594, 2001.

Thomason, L. W., and L. R. Poole, Use of stratospheric aerosol properties as diagnostics of Antarctic vortex processes, *J. Geophys. Res.*, *98*, 23,003–23,012, 1993.

Thomason, L. W., L. R. Poole, and T. Deshler, A global climatology of stratospheric aerosol surface area density derived from Stratospheric Aerosol and Gas Experiment II measurements: 1984–1994, *J. Geophys. Res.*, *102*, 8967–8976, 1997.

Tolbert, M. A., Sulfate aerosols and polar stratospheric cloud formation, *Science*, *264*, 527–528, 1994.

Toon, O. B., E. V. Browell, S. Kinne, and J. Jordan, An analysis of lidar observations of polar stratospheric clouds, *Geophys. Res. Lett.*, *17*, 393–396, 1990.

Toon, O. B., A. Tabazadeh, E. V. Browell, and J. Jordan, Analysis of lidar observations of Arctic polar stratospheric clouds during January 1989, *J. Geophys. Res.*, *105*, 20,589–20,615, 2000.

Voigt, C., et al., Nitric acid trihydrate (NAT) in polar stratospheric clouds, *Science*, *290*, 1756–1758, 2000.

Waibel, A., et al., Arctic ozone loss due to denitrification, *Science*, *283*, 2064–2069, 1999.

Waters, J. W., Microwave limb sounding, in *Atmospheric Remote Sensing by Microwave Radiometry*, edited by M. A. Janssen, chap. 8, pp. 383–496, John Wiley, New York, 1993.

Waters, J. W., An overview of the EOS MLS experiment, *Tech. Rep. D-15745, Version 1.1*, Jet Propulsion Laboratory, 1999.

Waters, J. W., et al., The UARS and EOS Microwave Limb Sounder (MLS) experiments, *J. Atmos. Sci.*, *56*, 194–218, 1999.

Wirth, M., A. Tsias, A. Dörnbrack, V. Weiss, K. Carslaw, M. Leutbecher, W. Renger, H. Volkert, and T. Peter, Model-guided Lagrangian observation and simulation of mountain polar stratospheric clouds, *J. Geophys. Res.*, *104*, 23,971–23,981, 1999.

World Meteorological Organization, *Scientific assessment of ozone depletion, 1998*, WMO Rep. 44, Global Ozone Res. and Monit. Proj., Geneva, Switzerland, 1999.

Zhang, R., P. J. Woodbridge, J. P. Abbatt, and M. J. Molina, Physical chemistry of the H_2SO_4/H_2O binary system at low temperatures: Stratospheric implications, *J. Phys. Chem.*, *97*, 7351–7360, 1993.

Zurek, R. W., G. L. Manney, A. J. Miller, M. E. Gelman, and R. M. Nagatani, Interannual variability of the north polar vortex in the lower stratosphere during the UARS mission, *Geophys. Res. Lett.*, *23*, 289–292, 1996.

M. L. Santee (corresponding author) and J. W. Waters, Jet Propulsion Laboratory, Mail Stop 183–701, 4800 Oak Grove Drive, Pasadena, CA 91109. (e-mail: mls@mls.jpl.nasa.gov)

E. J. Jensen and A. Tabazadeh, NASA Ames Research Center, Moffett Field, CA 94035.

G. L. Manney, Department of Natural Resources Management, New Mexico Highlands University, Las Vegas, NM 87701.

M. Fromm, Computational Physics, Inc., 2750 Prosperity Avenue, Fairfax, VA 22031.

R. M. Bevilacqua, NRL, Code 7227, Washington, DC 20375.

This preprint was prepared with AGU's LaTeX macros v4, with the extension package 'AGU++' by P. W. Daly, version 1.5g from 1998/09/14.